Available online at www.sciencedirect.com

ScienceDirect

journal homepage: www.elsevier.com/locate/he

Steam reforming of methanol over x% Cu/Zn–Al 400 500 based catalysts for production of hydrogen: Preparation by adopting memory effect of hydrotalcite and behavior evaluation

D. Hammoud [a,b,c], C. Gennequin [a,b,*], A. Aboukaïs [a,b], E. Abi Aad [a,b]

[a] Université Lille Nord de France, F-59000 Lille, France
[b] Université du Littoral Côte d'Opale, Unité de Chimie Environnementale et Interactions sur le Vivant, E.A. 4492, MREI 1, 59140 Dunkerque, France
[c] Conseil National de la Recherche Scientifique Libanais (CNRSL), Liban

ARTICLE INFO

Article history:
Received 19 June 2014
Received in revised form
8 September 2014
Accepted 15 September 2014
Available online 13 October 2014

Keywords:
H_2 production
Steam reforming of methanol (SRM)
Reconstruction
Cu/Zn–Al
Memory effect

ABSTRACT

A novel catalyst for hydrogen production from the catalytic process of methanol steam reforming could play an important role in hydrogen production to be used as a feed for fuel cell. Our study focuses on the preparation of copper supported on calcined hydrotalcite catalysts using the memory effect of zinc–aluminum hydrotalcite. Zinc–aluminum was calcined at 400 °C and dipped in a copper nitrate aqueous solution. The steam reforming of methanol was studied in a fixed-bed reactor under mild conditions and a reaction temperature range of 200–350 °C. The catalysts were characterized by XRD, SEM, TPR, chemisorption N_2O, TG/DTA, IR and N_2 adsorption techniques in order to identify their physical and chemical properties. The results evince the regeneration and the reconstruction of the layered structure that have a positive influence on the interactions between support and copper species. After activation by calcination at 500 °C, the solids copper/zinc–aluminum (Cu/Zn–Al 400 500) showed an interesting mixed oxides and were tested in the reaction of methanol steam reforming. The 10% Cu/Zn–Al 400 500 exhibits the best catalytic activity about 75.44% of H_2 yield with 51.87% of methanol conversion at 250 °C. Methanol conversion was found to be a strong function of catalyst reducibility and copper concentration. Also, reaction temperature depended strongly on the amount of Cu_2O formed in the activated catalyst.

Introduction

The growing world population leads to increase the demand of energy. To date, fossil fuels have been used as the main energy sources to support such demand. Unfortunately, fossil fuel reserves are expected to last no longer than 50–100 years. The shortage of energy is thus becoming a noticed problem for mankind, prompting worldwide searches for alternative energy resources [1].

* *Corresponding author*. Université Lille Nord de France, F-59000 Lille, France.
E-mail address: cedric.gennequin@univ-littoral.fr (C. Gennequin).
http://dx.doi.org/10.1016/j.ijhydene.2014.09.080

Energy from hydrogen feeding to a fuel cell is one of the most interesting alternative resources. A fuel cell unit generates electrical energy from an electrochemical reaction of hydrogen with oxygen, yielding an environmentally benign by product, water [2,3]. The hydrogen fuel cell is claimed as an alternative energy resource, with high efficiency [4]. In comparison with conventional internal combustion engines, fuel cells have been extensively studied due to their attractive properties, such as high power density, low emissions of pollutants, low temperature operation and compactness. The hydrogen used in fuel cells can replace fossil fuel. By combining the hydrogen with fuel cells, it can be efficiently used to convert the chemical energy into electricity. Among the various types of fuel cells, the polymer electrolyte membrane fuel cells (PEMFCs) are mostly used for small and medium sizes stationary and mobile applications.

The alternative to the use of either liquid hydrogen or high pressure hydrogen on board is to carry liquid fuels that have high energy densities and covert those to a hydrogen-rich gas (reformate) via an on-board fuel cell processor [5]. One of the most favorable liquid fuels used to produce hydrogen on board is methanol. This is due to the following superior advantages of using methanol in comparison to other liquid fuels in particular with respect to the on-board reforming process:

1. Low cost, boiling point, reforming temperature and atmospheric pressure.
2. Simple molecule with high molar ratio of hydrogen to carbon and as being easily stored.
3. Low CO concentration (CO is poison to the fuel cell performance).
4. No emission of pollutants, such as NO_x, SO_x.

For the purpose of fuel-cell application, H_2 can be extracted from methanol through different processes [6]: decomposition, steam reforming and partial oxidation. The two last reactions produce a considerable amount of CO as a by product. For the application of PEMFC, even traces of CO (>20 ppm) in the reformed gas deteriorate a Pt electrode and the cell performance is lowered dramatically. Hence, in order to utilize hydrogen for fuel cells, it is highly desirable to develop a process that can produce hydrogen without or with the minimum CO in the reformed gas. The reaction of steam reforming of methanol (SRM) is shown in equation (1) [7]. This reaction provides the highest hydrogen production among other reforming reactions.

$$CH_3OH + H_2O \rightarrow 3H_2 + CO_2 \quad \Delta H^0 = +49.4\ kJmol^{-1} \qquad (1)$$

In the literature, the most frequently tested catalysts for SRM belong to the $Cu–ZnO–Al_2O_3$ system, with quite high copper content (30–50 wt% as CuO). In most cases, the commercially available industrial low temperature water gas shift catalysts are tested for SRM [8], although they have been optimized for a different reaction. Hydrotalcite-type solids (Fig. 1) have been proposed as possible precursors for such catalysts. Hydrotalcite – like compounds, also known as layered double hydroxides (LDH) or anionic clays, have a layered structure derived from that of brucite, i.e. magnesium hydrotalcite. To understand the structure of these

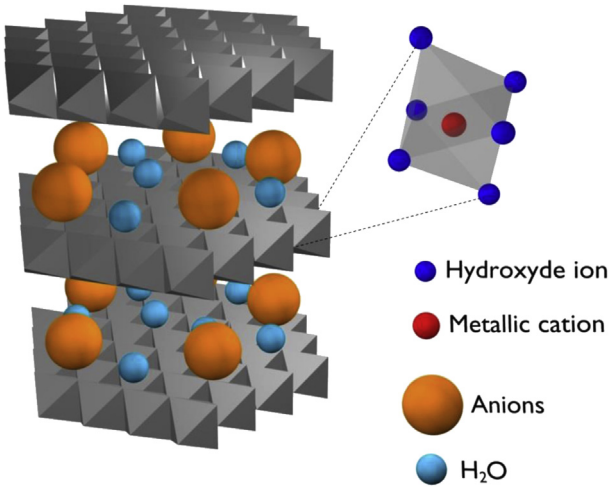

Fig. 1 – Structure of hydrotalcite.

compounds, it is necessary to start from the structure of brucite, $Mg(OH)_2$, where octahedron of Mg^{2+} (6-fold coordinated to OH^-) share edges to form infinite sheets. These sheets are stacked on top of each other and are held together by hydrogen bonding. When Mg^{2+} ions are substituted by a trivalent ion having not too different radius (such as Fe^{3+} for pyroaurite and Al^{3+} for hydrotalcite, respectively), a positive charge is generated in the hydroxyl sheet. This net positive charge is compensated for by CO_3^{2-} anions, which lie in the interlayer region between the two brucite-like sheets. In the free space of this interlayer the water of crystallization also find a place. The most interesting properties of the oxides obtained by calcination are the following [9]:

- High surface area,
- Basic properties,
- Formation of homogeneous mixtures of oxides with very small crystal size, stable to thermal treatments, which by reduction form small and thermally stable metallic crystallites,
- "Memory effect",

The calcination of hydrotalcite can lead foremost to the formation of amorphous compounds followed by pre-spinel oxides which can contribute to increase significantly the specific surface area. It is known that hydrotalcite have basic properties significantly lower than those of their mixed oxides obtained by the thermal decomposition. The basic properties of the decomposed phase depend on the report M^{II}/M^{III} and on the temperature of calcination. The basic sites are of type O^{2-}, $M^{2+}–O^{3-}$, $M^{2+}–O^{2-}$ and OH^-. In general, the carbonates affect the effective basicity of catalyst covering the most basic sites which are no longer available for a possible interaction with an acid reactant [9].

Ternary $CuO/ZnO/Al_2O_3$ catalysts have been widely employed in the actual reforming process since the early 1960s. The catalyst was usually prepared by a co-precipitation (cp-) method, resulting in the higher Cu metal dispersion and, as a consequence, the higher catalytic activity [10]. However, such type of catalysts are not sustainable enough in the

reformer for PEFCs, since the deactivation took place due to an oxidative sintering of Cu metal species especially during daily startup and shutdown operation, which is inevitable for the domestic use. We have applied an impregnation method of copper solution on calcined support synthesized by hydrotalcite route.

Few papers have reported the modification of Cu/ZnO/Al_2O_3 catalysts by adopting a "memory effect" of hydrotalcite that is the recovery of the original layered structure of LDH from ex- LDH [11], possibly formed in the catalyst precursors. As a result of the contact of the catalyst oxide form with water, complex physicochemical processes occur, leading to the reconstruction of the layered structure. As long as the temperature of the thermal treatment of the LDH material is lower than the critical value [9], this structural memory effect is feasible. Too high temperature results in the formation of stable, highly crystalline oxide and spinel forms, from which the HT-like structure cannot be recovered.

In the present work, we aim to study the performance of various copper contents impregnated on Zn–Al–O mixed oxides derived from the Zn–Al hydrotalcite by adopting the "memory effect" for the steam reforming of methanol (1). Besides, the results of this study could lead to a better understanding of the influence of catalyst preparation in order to develop efficient catalyst for hydrogen production from the steam reforming process.

Materials and methods

Preparation of catalysts

$Zn_6Al_2(OH)_{16}CO_3{\cdot}4H_2O$ precursor was prepared, respecting the ratio with $M^{2+}/M^{3+} = 3$, via hydrotalcite route by co-precipitation (cp) as follows: an aqueous solution of $Zn(NO_3)_2{\cdot}6H_2O$ and $Al(NO_3)_3{\cdot}9H_2O$ was dropped into an aqueous solution of Na_2CO_3 with vigorous stirring and the pH was simultaneously adjusted to 10 by addition of an aqueous solution of NaOH (2 M) at 60 °C. The solution containing the precipitate was aged at 60 °C for 1 h then dried for 24 h. The obtained precipitate was filtered, washed with distilled water (50 °C) and dried at 60 °C for 48 h. After that, it was calcined at 400 °C under a flow of air to form the oxide of zinc aluminum denoted Zn–Al 400 [12].

Copper impregnation has been done by adopting the "memory effect" of Zn–Al hydrotalcite as follows: 1.0 g of the powder Zn–Al calcined at 400 °C were dipped in 100 ml of aqueous solution of copper nitrate $Cu(NO_3)_2{\cdot}3H_2O$ with different percentage weight x (x = 1, 2, 5 and 10) for 1 h under agitation at room temperature. This process was followed by the drying treatments: first with a rotary evaporator, then in a furnace with low humidity environment at 60 °C for 24 h. During the dipping, Zn–Al hydrotalcite was reconstructed from Zn–Al–O mixed oxide due to the "memory effect". The samples were finally calcined at 500 °C under flow of air (33 ml min^{-1}, 1 °C/min, and 12 h at 500 °C) and were denoted x % Cu/Zn–Al 400 500.

Several physicochemical techniques as XRD, FT-IR, SEM, TG-DTA, BET, N_2O chemisorption and TPR were used to characterize the synthesized catalysts.

Characterization

Powder X-ray diffraction (XRD) patterns were measured on a Brüker D8 advance diffractometer equipped with a copper anode (λ = 1.5406 Å). The samples were scanned between $4° < 2\theta < 80°$ with the step size of $\Delta(2\theta) = 0.02°$ and a count time/step = 6 s. The comparison with the JCPDS files allows the indexing of the diffraction patterns.

Coupled thermogravimetric (TG) and differential thermal (DTA) analyses were performed with a Netzsch STA 409 apparatus equipped with a microbalance in a flowing air. Approximately 25 mg of sample was heated in an open platinum crucible in air stream flow of 75 ml min^{-1}, raising the sample temperature to 1000 °C.

The IR absorption spectra were recorded with an FT-IR Equinox 55 Brüker spectrometer in the range 4000–400 cm^{-1} and a resolution of 4 cm^{-1}. For the analysis of the skeletal vibrations, KBr pressed disks were used. The "operando" FT-IR spectra were recorded using a diffuse reflectance accessory equipped with a high temperature cell (Harrick accessories). The solid was heated under air from the ambient temperature till 400 °C and the spectra were registered in function of temperature in the range 4000–1000 cm^{-1} with 32 scans and a resolution of 4 cm^{-1}.

The morphology of powder is examined with a 438 VP microscopy (LEO Cambridge). The samples were metallized with gold–palladium.

BET surfaces of the samples were determined by nitrogen adsorption at −196 °C (using thermo-electron Q surf M1 apparatus) preceded by outgassing for 30 min at 130 °C. The surface areas were calculated according to the method of Brunauer, Emmett and Teller (BET).

The study of porosity was measured on Sorptomatic 1990 (Thermo Electron Corporation). The sample should be treated under vacuum to remove all the impurities. It was heated at 350 °C to liberate pores from water and impurities. Then it was dipped in liquid nitrogen at −196 °C and analyzed to determine the volume of adsorbed nitrogen.

An Altamira AMI 200 apparatus equipped with a TCD detector was employed for TPR measurements. A pretreatment of the sample under a flow of argon at 150 °C during 1 h is recommended. TPR analyses were carried out on calcined samples at a rate of 5 °C.min^{-1} using a 5% H_2/Ar (30 ml.min^{-1}) mixture from 20 to 900 °C.

The N_2O-measurements are made at ambient pressure, prior to each measurement, the sample was pretreated with argon at 150 °C. Then a reduction with H_2/Ar at 700 °C was occurred. The reactor is then cooled for the N_2O reaction and then flushed with argon at 90 °C. A measurement is initiated by switching from argon to N_2O at 90 °C to oxidize copper at surface of catalysts followed by flow of argon. A second TPR from 90 to 400 °C is realized to reduce the copper oxidized at the surface. The amount of N_2O evolved can be accurately computed from the H_2-back-titration.

Experimental conditions of tests

The catalyst was pretreated in a flow of argon (25 ml.min^{-1}) at 200 °C for 2 h. A long-shaped Pyrex glass tube with an inner diameter of 8-mm was used as a reactor. Typically a 70–80 mg

portion of catalyst was loaded into the reactor with a coaxially centered thermocouple. The SRM reaction was carried out using a fixed-bed flow reactor in the temperature range 200–350 °C at atmospheric pressure with $H_2O/CH_3OH = 2$. The reaction was started by introducing the reactants to the reactor (0.8 ml.h^{-1}) into the preheater carried by argon (25 ml.min^{-1}) by means of a liquid pump. All the lines and valves through the reactants feed, the entry; the exit of the reactor and the gas chromatographs were heated to 160 °C to prevent the condensation of water. The reaction was carried out under stepwise increasing temperature from 200 to 300 °C during 3 h. The outflow gases were automatically analyzed by on-line gas chromatograph (GC: Varian 3800). This GC was equipped with Haysep Q (CO_2, CH_4) and molecular sieve (H_2, CO), Ar carrier gas and TCD. Also, the by products: formaldehyde (HCHO), formic acid (HCOOH) and methyl formate (CH_3OCHO) were analyzed by FID of the GC. This first heating is intended to activate catalyst and identify the oxidation state of copper after reaction. Copper species were reduced by H_2 produced during reaction and simultaneously undergone a reoxidation in the vaporized feed containing water.

The conversion of methanol and the selectivity of different products were calculated by the following formulas:

$$\text{Conversion}(\%) = 100 * \frac{n^0_{MeOH} - n^f_{MeOH}}{n^0_{MeOH}}$$

$$\%SH_2 = \frac{100^* \text{ molarity of } H_2}{\sum \text{products of the reaction}}$$

$$\%SCO_2 = \frac{100^* \text{ molarity of } CO_2}{\sum \text{products of the reaction}}$$

$$\%SCO = \frac{100^* \text{ molarity of CO}}{\sum \text{products of the reaction}}$$

The catalysts were characterized after activation by several methods (XRD, N_2O chemisorption, TG/DTA and IR).

At low temperature, the conversion of methanol was absent without reduction, it may be due to the non-presence of the active species responsible of activation of reactants in absence of reduction. For that, the reduction and oxidation pre-treatment (first heating) was recommended to activate the catalyst at low temperature before starting heating again from 200 to 300 °C with the same steps mentioned above.

To follow the evolution of the non-converted reactants, products and by-products, we have coupled a mass spectrometry to the GC, this operation helps us to identify the mechanism reaction over the x% Cu/Zn–Al 400 500 catalysts.

Results and discussion

X-ray diffraction (XRD)

The diffractograms of the hydrotalcite Zn–Al HT and the calcined support Zn–Al 400 are presented in Fig. 2. The XRD pattern of Zn–Al HT showed the presence of two phases: hydrotalcite (JCPDS 37-0629) and $Zn(OH)_2$ (JCPDS 01-0360). After calcination at 400 °C, the hydrotalcite structure is not detected but the formation of ZnO was revealed in agreement with the file JCPDS 36-1451.

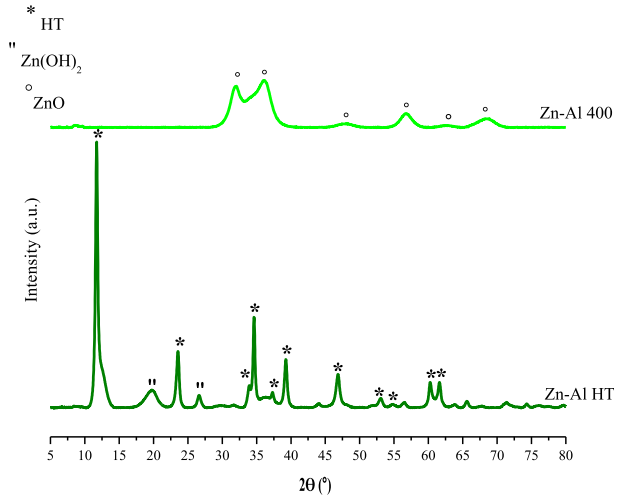

Fig. 2 – XRD patterns of Zn–Al HT and Zn–Al 400.

The XRD patterns of the four dried impregnated catalysts 1, 2, 5 and 10% Cu/Zn–Al 400 are reported in Fig. 3. For comparison, the XRD of the Zn–Al HT sample is also added. The support presents the sharp peaks of hydrotalcite phase (JCPDS 37-0629) at diffraction angles $2\theta = 11.6$, 23.3, 34.5 and 60.1° corresponding to the basal planes (003), (006), (009) and (110), respectively, with a good crystalline order and the phase of $Zn(OH)_2$ (JCPDS 01-0360) was detected. Furthermore, the patterns of impregnated samples show the formation of two distinct crystalline phases: ZnO (JCPDS 36-1451) and hydrotalcite. The presence of this latter phase is related to the regeneration capacity by "memory effect" of oxide derivative from hydrotalcite when it contacts a water solution containing various anions (hydration) and it depends on the previous calcination temperature. The easier reconstruction of the support is obtained when samples are calcined at low temperature [13].

The hydrotalcite phase (Fig. 1) in our samples is crystallized in rhombohedral 3R symmetry. Ions like Cu^{2+} form compounds characterized by the presence of cooperative Jahn-Teller

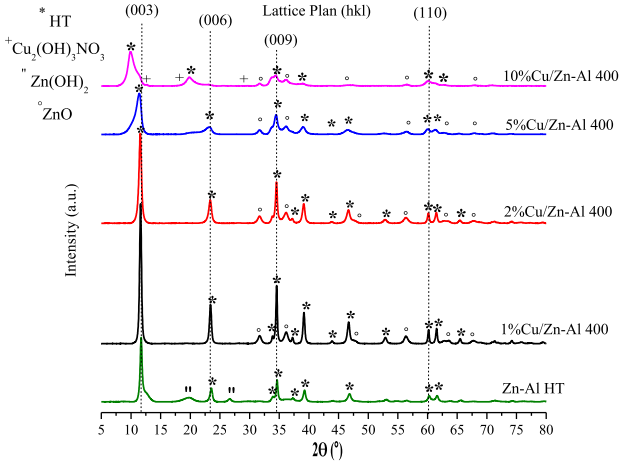

Fig. 3 – XRD patterns of Zn–Al HT and dried impregnated catalysts *x*% Cu/Zn–Al 400.

effect: the distortion in the octahedral coordination structure leads to a gain in energy. In the HT, until the Cu^{2+}/M(II) ratio is lower than or equal to 1, the Cu^{2+} cations in the brucite sheet are separate from one another, and copper arranges in an undistorted octahedral coordination typical of the brucite structure. When the ratio is higher than 1, the Cu^{2+} ions can be situated in near-lying octahedra, and the formation of the copper compound (with distorted octahedron) is energetically preferred to that of HT. The Al^{3+} ions in the brucite-like sheet remain distant one from the other, because of the repulsion of positive charges. According to Brindley and Kikkawa [14], for Al_x with x higher than 0.33, the increased number of neighboring Al octahedra leads to the formation of $Al(OH)_3$ (not detectable by X-ray measurements).

The parameters of the unit cell being a and $c = 3c'$ (where c' is the thickness of one layer constituted by a brucite-like sheet and one interlayer) calculated from the first basal reflection d_{003} and reported in Table 1 are similar to those reported in bibliography [9].

The number, the size, the orientation and the strength of the bonds between the anions and the hydroxyl groups of the brucite-like layers determine the thickness of the interlayer. This thickness is the difference between c' and 4.8 Å (thickness of brucite layer) [15]. As shown in Table 1, the values of c' correlated with the presence of several anions in interlayers such as OH^-, CO_3^{2-} and NO_3^-. The parameter c' observed with carbonate is related to the strong hydrogen bond that occurs in the carbonate-containing HT [16]. In addition, the low value of c' observed with OH^- is related to the similarity of its ionic diameter with that of the water molecule, and to the strong hydrogen bridges among the water and the OH^- of the basic layers; this leads to the best close-packed arrangement [15,17].

A partial reconstruction of hydrotalcite is suggested and a part of the samples remained as ZnO oxide, the patterns of the impregnated catalysts are not completely similar to the initial support Zn–Al HT and it was evidenced by the shift of $2\theta = 11.6°$. Nevertheless, we have noticed that the parameter d_{003} increases with the augmentation of the copper content x% in the samples, in parallel the peaks at 11.6° shifted to lower values (Fig. 3). This observation is due to the change of the ratio M^{2+}/M^{3+} supposed different from 3.

In addition, at low diffraction $2\theta = 11.6°$, an asymmetric shoulder is formed; it is probably caused by the heterogeneity of the layers in the regenerated hydrotalcite. During reconstruction process, a quantitative exchange of anions as like NO_3^- (from metal precursors) and OH^- (from water) with carbonate ions can be realized which leads to the mixture of the anionic interstitial layer and the apparition of the shoulder at 11.6°.

On the other side, the value of the parameter "a" is not affected by the nature of the anion; it depends on the distance between the cations. It is possible that anion exchange can take place during the reconstruction but the ionic radius of Cu^{2+}(0.69 Å) and Zn^{2+}(0.74 Å) have a small difference and the reconstruction was partial, for that no remarkable variation of the "a" values was noted (Table 1).

For 10% Cu/Zn–Al 400, a third phase is observed, it corresponds to the $Cu_2(OH)_3NO_3$ (JCPDS 75-1779).

During the aqueous impregnation by a copper solution on a Zn(Al)O oxide resulting from the calcination of a hydrotalcite, the reconstruction of the lamellar structure may be occurred by a mechanism of dissolution and recrystallization [18]. This mechanism involves though a cation exchange between the ions Zn^{2+} and Cu^{2+}. Thus it is possible to find several types of copper species dispersed on the support.

Table 1 – "a" and "c" parameters of dried impregnated x% Cu/Zn–Al 400 and comparison with literature.

Sample	d_{003} (Å) = c'	d_{006} (Å)	c_{003} (Å)	d_{110} (Å)	a (Å)
Zn–Al HT	7.544	3.774	22.632	1.5345	3.0690
1% Cu/Zn–Al 400	7.609	3.796	22.829	1.5366	3.0732
2% Cu/Zn–Al 400	7.641	3.804	22.924	1.5732	3.0746
5% Cu/Zn–Al 400	7.777	3.822	23.334	1.5399	3.0799
10% Cu/Zn–Al 400	8.091	4.466	24.274	1.5398	3.0797
Cu–Zn–Al LDH reference [9]	**7.665**	–	**22.995**	–	**3.073**
Zn–Al LDH reference [9]	**7.625**		**22.877**		**3.108**
CO_3^{2-}	**7.65**				
OH^-	**7.55**				
NO_3^-	**8.79**				

Scanning electron microscope (SEM)

The Zn–Al HT, Zn–Al 400 and x% Cu/Zn–Al 400 were characterized by SEM and showed in Fig. 4. The morphological feature of hydrotalcite is distinguished by the form of platelike expected from its layered structure (Fig. 4a). After calcination of Zn–Al at 400 °C, the lamellar structure was partially destroyed without maintaining the same morphology of the original precursor which evidenced the topotactical nature of the hydrotalcite decomposition step (Fig. 4b). After impregnation of different content of copper on Zn–Al 400, the samples consist of aggregates more or less developed platelet-shaped crystals with different dimensions. This effect can be attributed to the so-called "memory effect" of hydrotalcites. The samples with low content of copper (1 and 2% Cu/Zn–Al 400, Fig. 4c,d) show more lamellar structure than 5 and 10% (Fig. 4e, f) where the morphology was more compact which substantiate the reconstruction in different symmetries already discussed in XRD (shift of the first peak at $2\theta = 11.6°$).

Infrared spectroscopy (IR)

An infrared study of the vibrational structure of impregnated catalysts is presented in Fig. 5. For a better understanding of the heterogeneity of the layer thickness of regenerated hydrotalcite, the spectrum of Zn–Al HT is shown for comparison.

The structure of Zn–Al HT is formed by brucite-type layers (the same structure of brucite $Mg(OH)_2$) and the isostructural hydroxides of bivalent metals such as β-$Zn(OH)_2$ with carbonate ions in the interlayer region [19]. Obviously, there are two trivalent cations per carbonate ion. The water content is also related to the amount of trivalent cations. In the OH

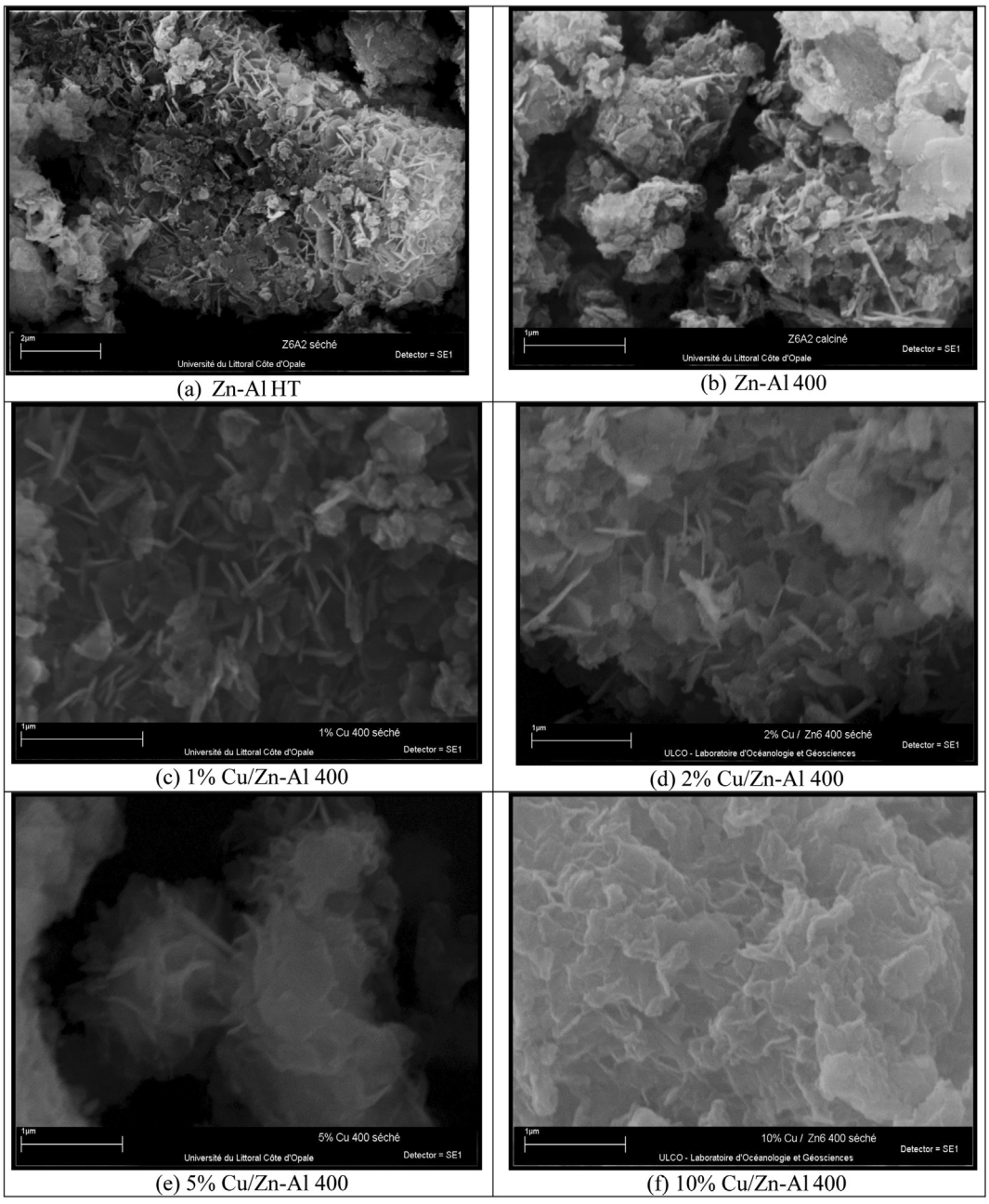

Fig. 4 – SEM images of (a) Zn–Al HT; (b) Zn–Al 400; (c) 1% Cu/Zn–Al 400; (d) 2% Cu/Zn–Al 400; (e) 5% Cu/Zn–Al 400; (f) 10% Cu/Zn–Al 400.

stretching region, three features in IR spectrum are expected, i.e. the antisymmetric OH stretching of the brucite-type layers and the antisymmetric OH stretchings of water molecules. The position and the shape of the OH stretching modes, centered at ~3450 cm^{-1}, is such that weak H-bonding do likely occur. The presence of water molecules is evidenced by the broad OH stretching band in the region 3150–2650 cm^{-1} and the H_2O scissoring mode band at 1630 cm^{-1}. The lack of multiplicity of the strong band at 1359 cm^{-1}, sharp and antisymmetric stretching of the carbonate ions, provides evidence in this case of the full absence of nitrate ions, which may remain as residuals of preparation salts.

The skeletal IR spectrum of Zn–Al 400 (Fig. 5) shows well evident bands at 791, 698 and 488 cm^{-1}. The typical doublet at 791 and 698 cm^{-1} is due to the vibrations of "isolated" MO_4 tetrahedra [20,21]. This material is actually a largely amorphous structure with some kind of intergrowth between the wurtzite and the spinel phase. The ZnO wurtzite structure has the hexagonal close packing of oxide ions and should form more complex structures when combines with $ZnAl_2O_4$ spinel. We can mention that, in this respect, the Zn–Al system differs from the Mg–Al system, the MgO structure (periclase or rock-salt) has the same oxygen packing of $MgAl_2O_4$ spinel (cubic close packing) and easily form solid solutions with it

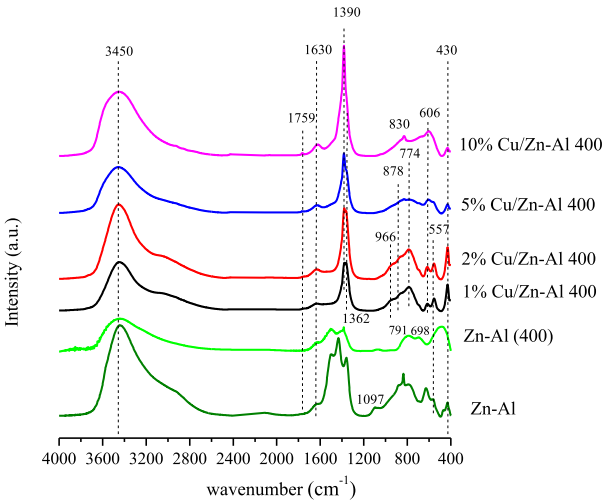

Fig. 5 – Skeletal IR spectra of Zn–Al, Zn–Al 400 and dried impregnated catalysts *x*% Cu/Zn–Al 400 (KBr pressed disk).

[19]. In addition, the bands observed between 1390 and 1500 cm^{-1} can be associated to the presence of remaining carbonates which means that the decarbonization of the hydrotalcite structure is not complete. This result is in accordance with the observations of SEM.

These latter results confirm the hypothesis of the presence of carbonate species highly coordinated to metallic centers with mono and bi-dentate bonds and probably located as oxy-carbonates. However, these latter may exist in weak concentrations or may be amorphous and escape the detection of XRD. The presence of oxy-carbonates facilitates the phenomena of reconstruction of hydrotalcite structure already described in the paragraph 3.1. In fact, the presence of water during the impregnation and the presence of residual carbonates on the support are sufficient to reform the lamellar structure. The regeneration of hydrotalcite from its oxide is possible and often known as "memory effect".

After impregnation of copper on the support Zn–Al 400, the samples were characterized by IR. For 1 and 2% Cu/Zn–Al 400, the weak asymmetric stretching mode of the carbonate ions is found at 1362 cm^{-1} but clearly presents a shoulder at higher frequency, near 1390 cm^{-1} detectable also for 5 and 10% Cu/Zn–Al 400. The apparent splitting of this degenerate asymmetric stretching mode of the carbonate ion may be due to the strong decrease in symmetry down to C_{2V} or lower, as proposed by Frost et al. [22]. Some heterogeneity of the neighboring of still highly symmetric carbonate ions is more likely, possibly due to a non-completely random distribution of carbonate and water in their interlayer positions, or due to more than one crystallographic site for their positions [8].

The carbonate ions should also give rise to other modes: the out-of-plane (oop) and the in-plane (ip) deformation. The positions of these modes is quite constant in carbonate minerals in the ranges of 820–900 (879 cm^{-1} for the free ion, oop) and 650–770 (680 cm^{-1} for the free ion, ip) [23]. A component is found near 878 cm^{-1} which is prominent and can be assigned to the out-of-plane deformation (oop) mode.

For the OH bending and metal oxygen vibrations of the "brucite-type" layers, several IR active modes may exist. Two transversal (TO) and longitudinal (LO) modes form the IR modes. For brucite-type hydroxides, the lattice vibrations with the symmetry E_u is expected to be strongly coupled with the deformations of the OHs ("librations", E_u) [8]. The band observed at 774 cm^{-1} and the shoulder distinguished at 966 cm^{-1} are attributed to the TO and LO components of the E_u deformations of the OHs that may have a relevant TO/LO splitting [24]. The strong doublet with the components at 557 and 430 cm^{-1} can be due to the lattice modes metal-oxygen with E_u symmetry. The band at 430 cm^{-1} is an overlapping of vibrations attributed to Al–O, $[AlO_6]^{3-}$ translations or Zn–OH [confirmed by the presence of the phase $Zn(OH)_2$ detected in XRD (Fig. 3)] [25].

Thermal analysis (TG-DTA)

The DTA curves show the typical features of the thermal decomposition of hydrotalcite phase in function of temperature (Fig. 6). Three endothermic peaks marked A, B and C are clearly observed. In the literature [25], the decomposition of hydrotalcite occurs in four steps. The first one, attributed to the loss of physisorbed water, occurs below 70 °C and correlated to peak A. The second step, situated between 150 and 200 °C, is broad and can be attributed to the loss of water cointercalated with anions in the hydrotalcite phase. It is associated to peak B. Peak C, observed between 200 and 280 °C, combines two steps: 3 (dehydroxylation of brucite layer) and 4 (loss of interlayer anions (carbonates, nitrates)) which are difficult to separate by DTA due to their close temperatures. At 700 °C, only a mixture of Zn and Cu oxides is present [19]. In addition, the loss of residual surface carbonate anions and/or dehydroxylation water can be observed around 600 °C [26,27].

On the other side, with increasing the content of copper impregnated, the thermal stability increases by shifting the destruction of the structure at higher temperature whence the 10% Cu/Zn–Al 400 is the most stable. For this catalyst, the shoulder observed at 230–250 °C may be due to the disappearance of NO_3^- related to $Cu_2(OH)_3NO_3$ shown in XRD and it

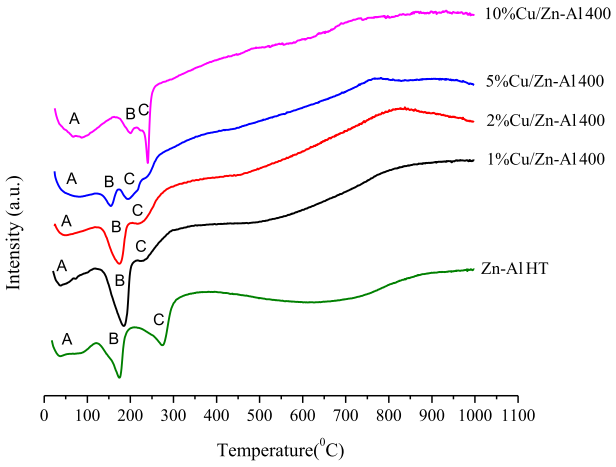

Fig. 6 – DTA signal of Zn–Al HT and dried impregnated catalysts *x*% Cu/Zn–Al 400.

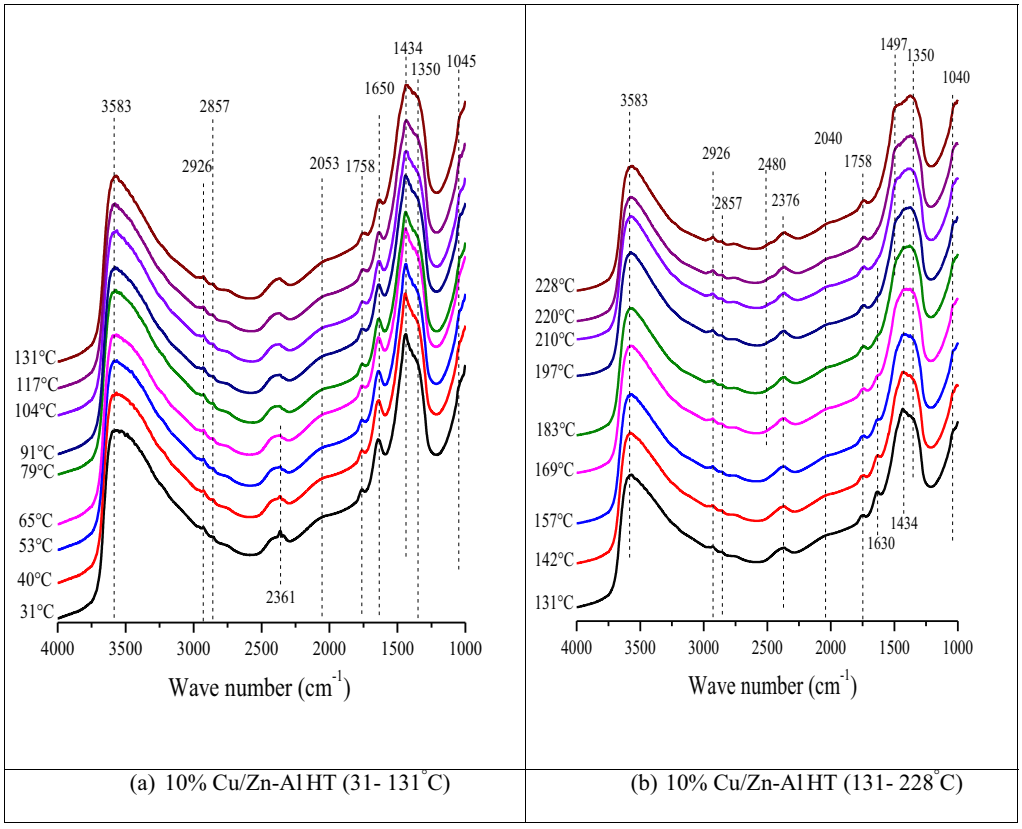

Fig. 7 – In situ DRIFTS of 10% Cu/Zn–Al 400 as function of temperature.

is destroyed at high temperature. The collapse of the hydrotalcite structure leads to the formation of metal oxides and the destruction of hydrotalcites means the departure of water molecules and CO_2.

Diffuse Reflectance Infrared Fourier Transform Spectroscopy (DRIFTS)

To have more details on the thermal destruction of impregnated catalysts, a follow of calcination of 10% Cu/Zn–Al HT by a Diffuse Reflectance Infrared Fourier Transform Spectroscopy (DRIFTS) was carried out. This study aims to identify the evolution of characteristic bands of regenerated hydrotalcite during calcination in air from ambient temperature till 440 °C (Fig. 7).

The results show a vibrational band at 3450 cm^{-1}, which is attributed to OH stretching vibrations of hydroxyl groups in the interlayer related to Cu, Zn and Al, and physically adsorbed water. The shoulder present at lower wave number (~3150 cm^{-1}) is induced by hydrogen bonding of H_2O to CO_3^{2-} ions in the interlayer space. The corresponding HOH bending vibration of interlayer water strongly coordinates to a cation not incorporated in the hydrotalcite structure and located at 1758 cm^{-1}. Another band at 1630 cm^{-1} may be due to HOH bending of physically adsorbed water [28] or to H_2O bending vibration of interlayer [29].

The intensities of the interlayer water bands at 3150 and 1630 cm^{-1} gradually decrease with increasing temperature. This means that increasing amounts of interlayer water in the Cu–Zn–Al–CO_3 LDH are removed with increasing temperature.

The presence of carbonate species is revealed by the band at 1350 cm^{-1} which persists till 298 °C then it shifts towards a lower wave number (1302 cm^{-1}). The state of CO_3^{2-} in the hydrotalcite is distinctly different according to nature of metals which constitute the structure. Another band centered at 1434 cm^{-1} corresponding to the CO_3^{2-} ν_3 begins to decrease in size as temperature increases and disappears at 197 °C. Gradually a band at 1497 cm^{-1} attributed to carbonate begins to appear at this temperature. This band diminishes as the temperature increases; this is to be expected at the amount of interlayer water diminishes and as a result, the entity of CO_3^{2-} begins to interact more strongly with the backbone of the hydrotalcite itself. All these information obtained from vibrational bands signify a rearrangement in the hydrotalcite structure during calcination leading to its destruction.

Calcination of solids at 500 °C and catalytic tests of steam reforming of methanol

Surface area and porosity

The N_2 adsorption isotherms of Zn–Al 400 and 10% Cu/Zn–Al 400 500 are reported in Fig. 8. The two isotherms are of type III, according to the IUPAC classification. This type is associated to the solids which present macropores (size of pores >50 nm). The multilayers are formed even at low pressures due to the strong adsorbent/adsorbate interactions. The hysteresis is of type H3 and it can be attributed to a capillary condensation

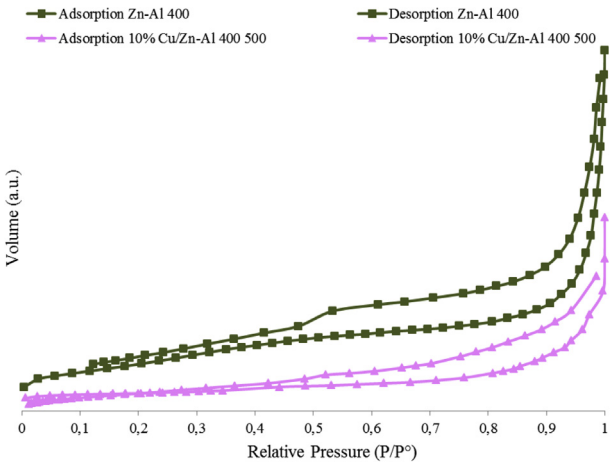

Fig. 8 – N_2 adsorption isotherms of Zn–Al 400 and 10% Cu/Zn–Al 400 500.

which occurred in a structure with pores in slot with non-uniform size [30]. This result is in agreement with those of scanning electron microscopy that showed for Zn–Al 400 a lamellar structure with the presence of sheets creating pores in the form of slots.

BET surface areas are presented in Table 2. The calcination of the support Zn–Al HT increases the specific area from 88 to 167 m^2/g due to the liberation of molecules of water and adsorbed species by outgassing and treatment. After impregnation of copper, the specific areas decrease for all the samples. These results are related to the structural change of oxide of zinc aluminum accompanying the regeneration of hydrotalcite phase. The evolution of specific surface may be explained by the possibility of formation of dense layer of hydrotalcite type on the surface which clogs the pores. On the other hand, the specific areas of all catalysts increase after calcination by clearing pores from water and impurities, as example, the 10% Cu/Zn–Al 400 500 recorded 42 m^2 g^{-1} instead of 9 m^2 g^{-1} when it was not calcined.

X-ray diffraction (XRD)

The regeneration of the hydrotalcite structure by "memory effect" is proved by several characterizations. The activation

Table 2 – Specific area, experimental weight loss and dispersion of different catalysts.

Samples	Specific area (m^2/g)	Experimental weight loss (%)	Dispersion (%)
Zn–Al HT	88	–	–
Zn–Al 400	167	–	–
1% Cu/Zn–Al 400	38	25.97	–
2% Cu/Zn–Al 400	51	26.19	–
5% Cu/Zn–Al 400	30	29.12	–
10% Cu/Zn–Al 400	9	31.99	–
1% Cu/Zn–Al 400 500	65	–	11.46
2% Cu/Zn–Al 400 500	81	–	15.80
5% Cu/Zn–Al 400 500	69	–	14.29
10% Cu/Zn–Al 400 500	42	–	8.47

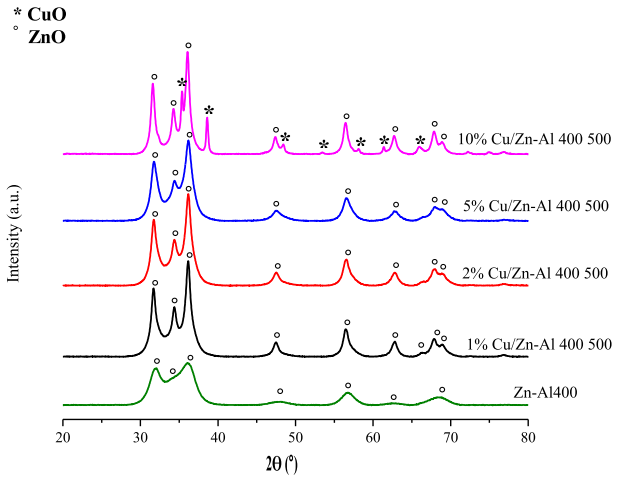

Fig. 9 – XRD patterns of calcined support and impregnated samples x% Cu/Zn–Al 400 500.

of solids is realized by calcination of dried impregnated x% Cu/Zn–Al 400 at 500 °C to form CuO oxides which will participate in the catalytic activity. XRD patterns of impregnated catalysts and calcined support are reported in Fig. 9. Crystallization of ZnO is present in all samples; while no phases containing aluminum are initially detected. After decomposition of the hydrotalcite phase, aluminum tends to remain in a mixed oxide phase, which is amorphous at 400 °C. Only for 10% Cu/Zn–Al 400 500, CuO (JCPDS 48-1548) was detected with crystallite size = 49.8 nm.

IR study

The IR spectra of the support Zn–Al 400 and the calcined catalysts x% Cu/Zn–Al 400 500 are regrouped in Fig. 10. The water band observed at 1630 cm^{-1} is assigned to water chemisorbed at outer surfaces. Furthermore, the shoulder at 1496 cm^{-1} signifies a weak splitting of the carbonate ν_3 band indicative of rearrangements of carbonate ions after calcination [31]. Also, the weak band near 1069 cm^{-1}, assigned to the symmetric ν_1 mode of carbonate, is due to the lowered symmetry of the interlayer carbonate ions by interaction with neighboring atoms [32]. Besides, a very weak band around 791 cm^{-1} is probably assigned to absorption of spinel but the XRD pattern does not reveal a crystalline spinel phase at 500 °C, suggesting that they are either amorphous or poorly crystallized. So, there is no evidence to relate the band around 800 cm^{-1} for the spinel phase [31].

The transformation from the hydroxide phase to an amorphous oxide and further to CuO can be noticed from the changes in the spectral range 700–400 cm^{-1}. The adsorption band at 698 cm^{-1} is related to the so-called ν_1 and ν_2 vibrational modes of isolated AlO_4 or ZnO_4 [25]. The Cu–O vibration that confirmed the formation of CuO is not clearly visible at 494 cm^{-1} in the spectra of 10% Cu/Zn–Al 400 500 [33].

TPR measurements

The results of TPR measurements of the impregnated catalysts calcined at 500 °C are shown in Fig. 11. For all catalysts samples, several reduction peaks and shoulders were seen between 197 and 272 °C and these were attributed to the reduction of different copper species. Although ZnO was not reduced under our experimental conditions, partial reduction of surface ZnO which may lead to the formation of α-brass (a dilute alloy of zinc in copper) only a few layers thick on the copper crystallites during the catalyst reduction, cannot be ruled out. In fact, thermodynamic calculations [34] are in favor of such a hypothesis, showing that the equilibrium zinc content in a surface α-brass is about 5% during catalyst reduction at 300 °C.

All catalysts present reduction peaks with asymmetric shapes and shoulders towards higher temperature. This is may be due to overlapping of several elemental reduction processes arising from different Cu^{2+} species.

The TPR profile of pure CuO is characterized by a single peak reported at 271 °C [35]. The TPR profiles of the catalyst at lower content of copper (1 and 2% Cu) are represented by single and broad reduction peaks centered at temperatures 272 and 253 °C, respectively. On the other hand, the peak

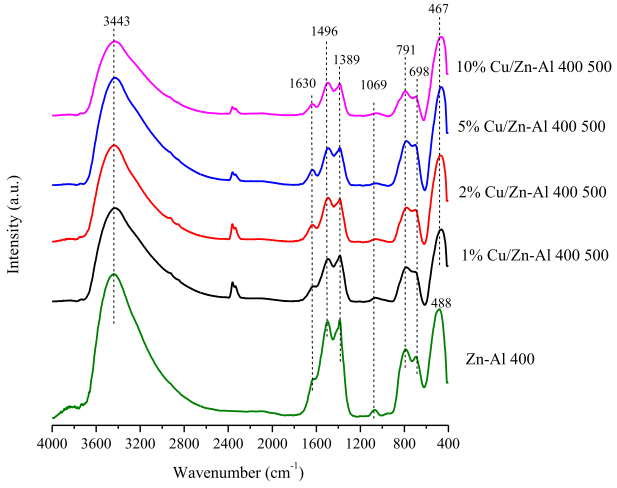

Fig. 10 – Skeletal IR spectra of Zn–Al 400 and calcined impregnated catalysts x% Cu/Zn–Al 400 500.

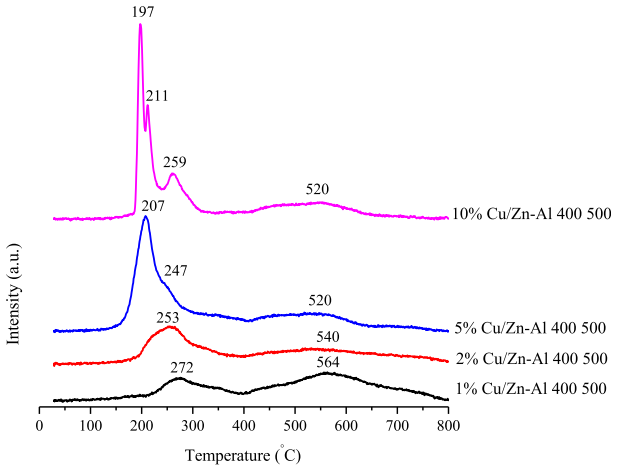

Fig. 11 – H_2-TPR profiles of impregnated catalysts x% Cu/Zn–Al 400 calcined at 500 °C.

shape in the TPR profiles of the catalysts at higher copper loading (5 and 10% Cu) is changed gradually. In fact, the TPR profile of 5% can be distinguished from 1 and 2% because, close to the prominent peak at 247 °C, a shoulder appears in the lower temperature side at 207 °C (Fig. 11). On increasing further the copper content to 10%, the intensity of the shoulder decreases and it is divided into two peaks, the first centered at 211 °C and the second at 197 °C.

In our investigated catalysts prepared by impregnation, the presence of ZnO affects the H_2 reduction of copper. First of all, the centered temperatures of reduction peaks in the TPR profiles of 2, 5 and 10% shift towards lower temperatures than the reduction temperature of pure CuO. This result points out that, ZnO certainly promotes the copper reduction and it plays the role of H_2 activator besides being a dispersive agent, thus enhancing the reduction of copper. It has been demonstrated that both the higher and the lower copper loading catalysts are formed by well-dispersed CuO–ZnO particles which are in intimate contact to each other [36,37]. It follows that the H_2 activation and spill over would be improved by this extended contact area between CuO and ZnO particles resulting in a promoting effect of the copper reduction. Therefore, we supposed that there are two reducible copper species in 5% Cu. One is represented by small CuO particles which are homogenously dispersed and are interacting with the ZnO particles; they reduce in correspondence of the peak around 247 °C and show reactivity similar in the 2% Cu but at higher temperature (253 °C). This suggests that dispersed CuO exists at low Cu (small dust) which is not detectable in XRD. The second type is represented by copper which experience even more enhanced reduction peak. These copper species are more reactive because they are in contact with the surface of the ZnO particles resulting in a strong interaction with them [35]. Particularly, the minor TPR peak observed at 197 °C is caused by presence of granular CuO (probably formed by the calcination at 500 °C of the phase $Cu_2(OH)_3NO_3$ detected by XRD (Fig. 3)) in 10% Cu/Zn–Al 400 500 [32]. Besides different copper species such as CuO, $CuAl_2O_4$ and Cu^{2+} incorporated in octahedral sites of the Al_2O_3 phase, some Cu (II) may exist as vicariant species in the zinc oxide and zinc aluminate. These species should be reduced at temperature higher than that of CuO [38] and could be related to the small signal that appears at about 570 °C in TPR profiles. The shoulder observed in 5 and 10% Cu may be rather attributed to the formation of Cu(I) as an intermediate in reduction of impregnated catalysts.

The step of the reconstruction is very important and the degree of copper and zinc exchange influences the nature, the dispersion of the copper species on the support and their interaction with Zn and/or Al. Thus, the reconstruction of the support can generate high quantity of active surface copper species.

Catalytic activity measurements for the steam reforming process

The performance of the catalysts for the steam reforming of methanol is listed in Table 3. At 200 °C, all the catalysts were active after reduction pre-treatment. When comparing the conversion of the best catalysts, it is evident that the 10% Cu/Zn–Al 400 500 has the highest conversions at 250, 300 and 350 °C followed by the 5% Cu/Zn–Al 400 500 (Fig. 12). At 350 °C, methanol conversion in presence of 10% Cu reaches 99.78% and the hydrogen selectivity 75.07% is equal to the theoretical stoichiometric of the reaction. Moreover, the formation of CO begins at 300 °C and it rises with increasing temperature but never exceeds 1.74% (Table 3). The lowest conversion was obtained for 1% Cu/Zn–Al 400 500.

Our study indicates that the increase in methanol conversion with copper dispersion was not significant since the 10% Cu presents the best methanol conversion without having the best copper dispersion (Table 2). Contrariwise, dispersion of the catalytically active metal appears to affect the selectivities of reaction products. In 10% Cu, the formation of large crystallites of CuO which were detected by XRD prevents the good dispersion of copper and leads to the formation of CO at high temperature.

To understand the behavior of catalysts, we studied in details the reducibility of copper which affects interestingly the methanol conversion. It was noticed that methanol conversion increases as catalyst reducibility increases. Catalyst reducibility seems to be a more useful parameter than copper load alone because it takes into account the effects of both copper content and calcination temperature.

A deconvolution of the best catalyst 10% Cu was realized between 150 and 400 °C, the zone area of steam reforming of methanol (Fig. 13). The percentage of copper species reduced at each centered temperature was calculated by a deconvolution method and the results are the following: 32.1% at 197 °C, 29.8% at 211 °C and 38.1% at 259 °C. The high percentage of copper reduced till 211 °C (61.9%) is the reason of the best activity of 10% Cu versus the remaining catalysts.

To evidence the necessity of activation of catalysts by pre-treatment and to determine the oxidative state of copper after pre-treatment, TPR and XRD analysis of activated catalysts were performed.

Two peaks are observed in TPR profile of 10% Cu/Zn–Al 400 500 after activation (Fig. 14). The first one at 144 °C may be due

Table 3 – Conversion and selectivities of CO_2, H_2 and CO versus temperature of the impregnated *x*% Cu/Zn–Al 400 500 catalysts after reduction.

	200				250				300				350			
Catalysts	S_{CO}	S_{CO_2}	S_{H_2}	Conv	S_{CO}	S_{CO_2}	S_{H_2}	Conv	S_{CO}	S_{CO_2}	S_{H_2}	Conv	S_{CO}	S_{CO_2}	S_{H_2}	Conv
1% Cu/Zn–Al 400(500)	–	–	3.81	9.37	–	–	19.02	12.37	–	22.86	75.49	32.12	0.23	23.6	75.14	65.99
2% Cu/Zn–Al 400(500)	–	–	74.47	1.79	–	23.42	74.48	21.68	0.15	23.88	75.01	58.56	0.47	24.03	75.31	88.33
5%Cu/Zn–Al 400(500)	–	21.17	71.5	12.62	–	23.47	75.35	33.74	0.18	24.29	75.12	75.11	0.86	24.54	74.57	99.55
10% Cu/Zn–Al 400(500)	–	22.51	74.08	8.24	–	23.82	75.44	51.87	0.39	24.01	75.19	92.80	1.74	23.17	75.07	99.78

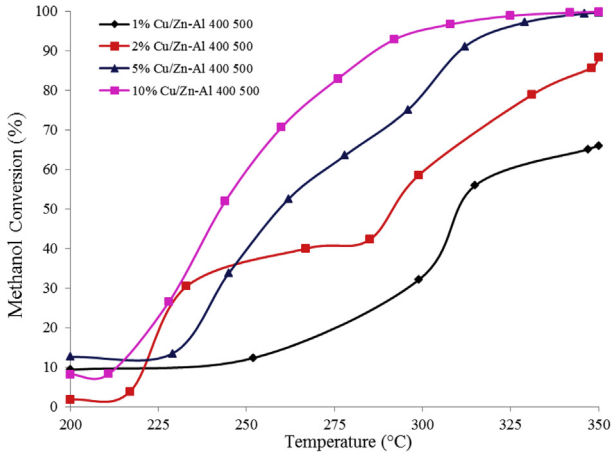

Fig. 12 – Curves of methanol conversion versus temperature of the impregnated catalysts x% Cu/Zn–Al 400 500, catalyst: 70–80 mg; flow rate: 0.013 ml.min^{-1}; H_2O/CH_3OH = 2.

to the reduction of Cu^{2+} species. The other peak at ~195 °C is characteristic of Cu_2O [39]. The amount of copper reoxidized to Cu_2O was calculated from H_2 consumption in the TPR experiments. XRD pattern corroborates the results of TPR (Fig. 15); it revealed the presence of Cu^0, ZnO and Cu_2O phases. This latter phase was absent or not detected in remaining catalysts. These results show that the activated catalysts required the combination of Cu^0 and Cu^{+1} together and may be Cu^{2+} because the first peak reduced at 144 °C in 10% Cu after activation was not observed in the other catalysts. Also, the catalytic activity depends on the composition of these elements in the catalyst. It was reported that methanol conversion increases with the amount of Cu_2O species.

It has been mentioned in literature that an induction period was needed before the catalysts became active. This observation suggests that the Cu^{+1} and Cu^0 species present at 200 °C (during first heating) have a low activity, for that no methanol conversion was observed. However, during the induction period, a fraction of Cu^0 was reoxidized to Cu_2O as it

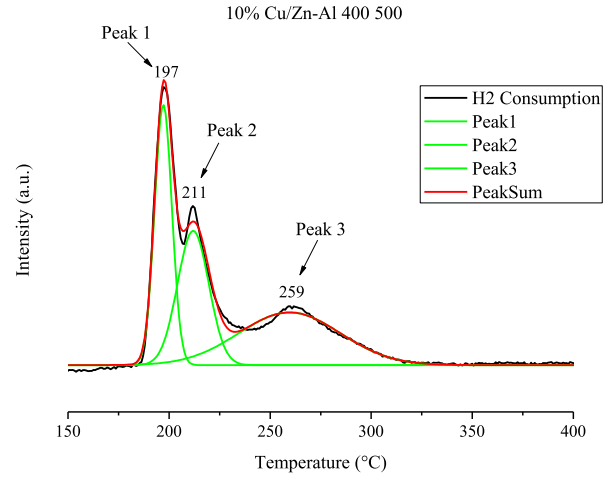

Fig. 13 – TPR deconvolution versus temperature of 10% Cu/Zn–Al 400 500.

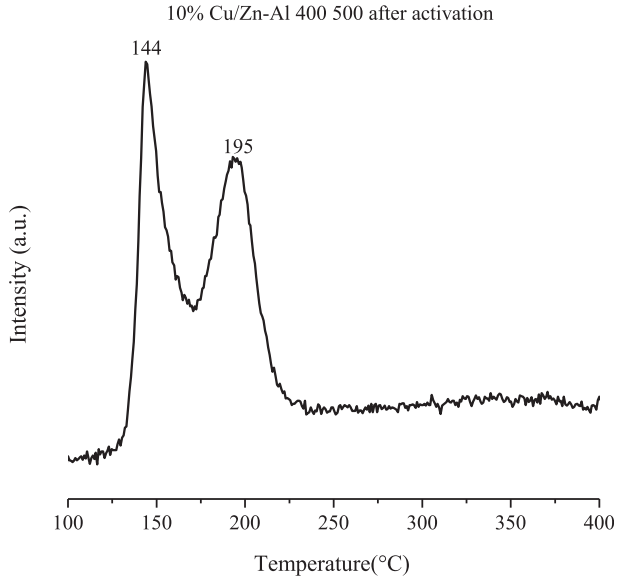

Fig. 14 – TPR profile of 10% Cu/Zn–Al 400 500 after activation (First heating).

was indicated earlier (Section experimental conditions of tests) [39]. The CO_2 produced during reaction and water reactant are responsible of the reoxidation of Cu^0 to Cu^{+1}.- Therefore, the induction period could be taken as the time required to produce an appropriate and active combination of Cu^0–Cu_2O for the reaction.

Products distribution

The products obtained from steam reforming of methanol in presence of impregnated catalysts are H_2, CO_2, CO, methyl formate (CH_3OCHO), HCHO and HCOOH.

Although the first attempt at elucidating the nature of methanol reforming mechanisms over various Cu-based catalysts was conducted nearly three decades ago, the active sites for H_2 production from methanol reforming are always controversial. Various mechanisms have been proposed regarding different states such as metallic Cu^0, or partially reduced Cu^{+1} or Cu^0–Cu^{+1} couple.

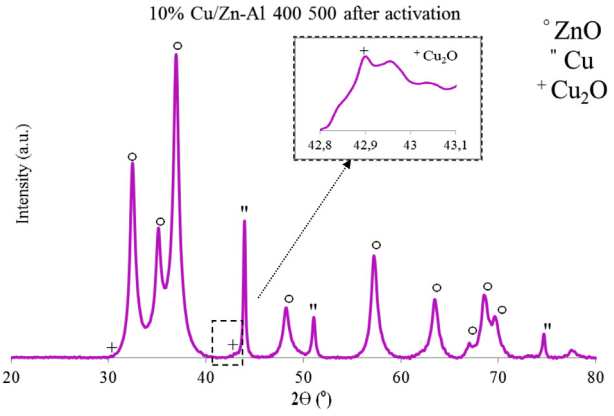

Fig. 15 – XRD pattern of 10% Cu/Zn–Al 400 500 after activation (First heating).

Four reactions schemes can be proposed for steam reforming of methanol and these schemes may be further complicated by the integration of carbon formation during the reaction [40]:

1 MD-WGSR,
2 1-step SRM,
3 SRM-MD-reverse-WGSR,
4 Methyl formate,

The MD-WGSR [41] proposed the CO as primary product formed from methanol dehydrogenation which was converted into CO_2 via WGSR. In the 1-step SRM scheme [6,42], the dehydrogenation of methanol produced CO_2 and H_2. Also the formation of CO appeared at temperature above 300 °C and became significant when methanol was totally converted. Agrell et al. concluded that CO production from the reverse-WGSR can be obstructed by a short residence time in the catalyst bed [43]. On the other hand, Peppley et al. claimed that the entire MD, WGSR and SRM participated in the reaction network [6,44]. They suggested that SRM and MD (a side reaction) occurred in parallel and the products of SRM are consecutively consumed in reverse-WGSR. This model required the presence of two distinct types of catalyst sites: one for both the SRM and reverse WGSR and second for the MD.

The temperature dependence of the product distribution results in presence of 10% Cu/Zn–Al 400 500 is shown in Fig. 16. The production of both CO_2 and H_2 increases with temperature whereas the formation of CO occurs above 250 °C (Fig. 16a). At the same time, if we follow the evolution of methyl formate CH_3OCHO, we can notice that its formation decreases above 250 °C (Fig. 16b). The formation of formic acid is weak at low temperature and a small quantity of formaldehyde is produced. Depending on our results, a part of our proposal reaction mechanism (Fig. 17) coincides with scheme 4 which was suggested by several researchers [45–47]. Two molecules of methanol dehydrogenate to form methyl formate which produces the formic acid by its reaction with water. The decomposition of formic acid produces CO_2 and H_2. These are the primary products of the system. The low amount of formaldehyde may result from the dehydrogenation of methanol. The other part of mechanism is determined by formaldehyde which intervenes in production of CO_2 and H_2. This supposition is released from the evolution of formaldehyde. Its formation, by dehydrogenation of methanol, increases gradually with temperature and it goes down above 300 °C, then it reacts with water and produces formic acid which decomposed to H_2 and CO_2. At the same time, the methyl formate almost disappears without canceling definitely its presence and giving the possibility of formation of formic acid that always persists at high temperature. Also, it is supposed in this period that the rate of the decomposition of methyl formate is slower than the dehydrogenation of formaldehyde.

Just at high temperature, the detected low CO concentration can be attributed to the reverse-WGSR, whereby CO was formed as secondary product. This could be due to the high concentrations of CO_2 and H_2 produced from the SRM. Its formation depends on the contact residence time.

Some researchers attributed the formation of methyl formate to the dimerization of formaldehyde. In contrast, other researchers disagreed on this route. A nucleophilic

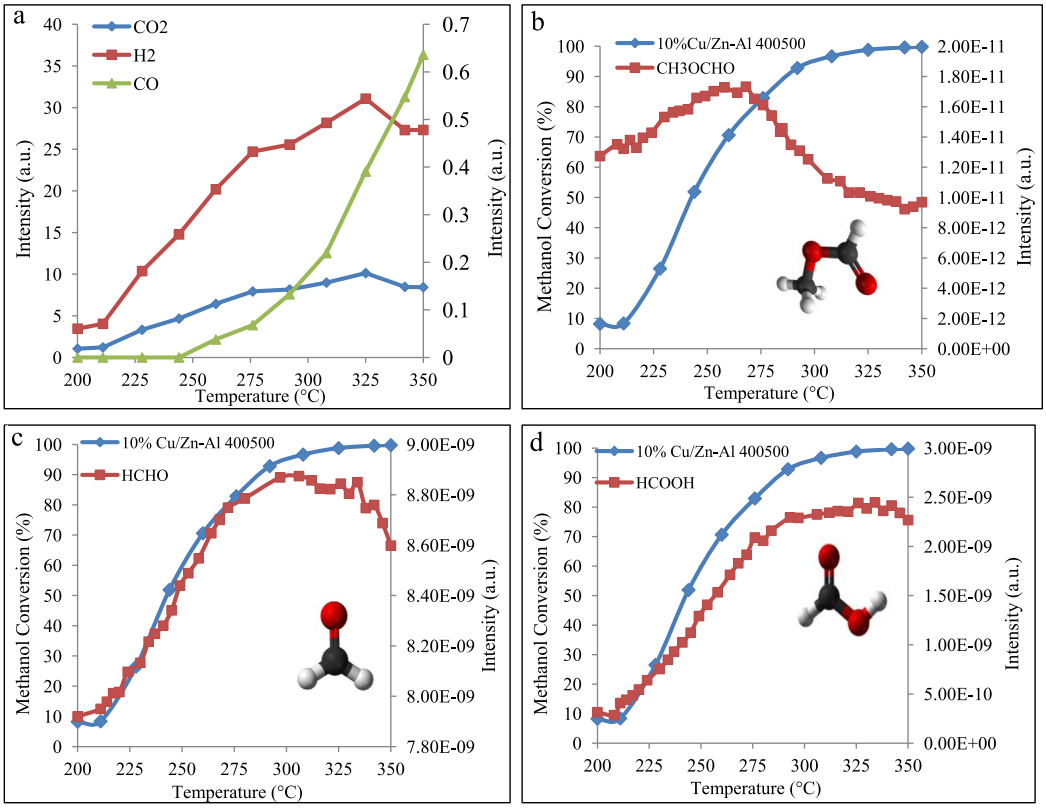

Fig. 16 – Evolution of products and by products of methanol steam reforming in function of temperature.

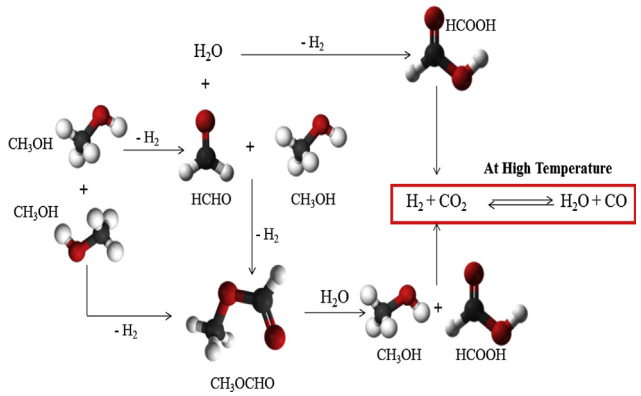

Fig. 17 – Suggestion of Reaction pathways of steam reforming of methanol.

transfer of H atom to carbonyl carbon in the formaldehyde molecule is involved in Tishenko mechanism [48]. This step requires the change of orbital configuration in formaldehyde from trigonal sp^2 to tetrahedral sp^3 which is not easy.

Conclusion

Impregnation of ex-HT mixed oxides by wet impregnation and with a carbonate–containing aqueous solution favors the HT recrystallization by "memory effect". The "memory effect" depends on both the impregnation solution and method besides the calcination temperature of the parent layered double hydroxide. The reformation of the HT phase was proved by XRD, TG/DTA, SEM and IR analysis. After calcination of x% Cu/Zn–Al 400 at 500 °C, the HT phase was destructed and interesting catalysts were generated with a high potential for H_2 production in steam reforming of methanol.

The results of catalytic tests indicate that 10% Cu/Zn–Al 400 500 is the most active for steam reforming. The conversion of methanol over the impregnated catalysts depends on the reducibility of copper species at low temperature and not on their dispersion because 10% Cu the best catalyst has the worst dispersion. Contrariwise, the dispersion influences the selectivities of products as the production of CO which was the highest for the best catalyst. Also reaction temperature had tremendous effect on selectivities. Therefore, it is so important to find a compromise between the dispersion and the reducibility of copper species with a good catalytic activity and low production of CO.

The characterizations after activation show that the catalyst activity depends on the formation of Cu_2O and Cu^0 species besides the possibility of remaining Cu^{2+}. Reaction efficiency was found to be strong function of the amount of Cu_2O formed in the activated catalyst and this amount depended on copper concentration.

HCHO, CH_3OCHO and HCOOH were also produced during steam reforming of methanol. A suggested mechanism of reaction was elaborated according to our observations. Till date, consensus on the surface reaction mechanisms involving steam reforming of methanol has not been established. Controversy should be resolved because mechanism can be useful for determining the role of the metal oxide, and ultimately for designing an optimal catalyst formulation.

Acknowledgment

The authors wish to thank the CNRSL for financing support and Dr. Lucie Courcot for her precious help in SEM analysis.

REFERENCES

[1] Shafiee S, Topal E. An econometrics view of worldwide fossil fuel consumption and the role of US. Energy Policy 2008;36:775–86.
[2] Zhang FY, Advani SG, Prasad AK. Performance of a metallic gas diffusion layer for PEM fuel cells. J Power Sources 2008;176:293–8.
[3] Kulikovsky AA. Direct methanol hydrogen fuel cell: the mechanism of functioning. Electrochem Commun 2008;10(9):1415–8.
[4] Edwards N, Ellis SR, Frost JC, Golunski SE, Keulen ANJ, Lindewald NG, et al. On-board hydrogen generation for transportation applications: the HotSpot methanol processor. J Power Sources 1998;781:123–8.
[5] Nishida K, Atake I, Li D, Shishido T, Oumi Y, Sano T, et al. Effects of noble metal-doping on $Cu/ZnO/Al_2O_3$ catalysts for water-gas shift reaction: catalyst preparation by adopting "memory effect" of hydrotacite. Appl Catal A *Gen* 2008;337:48–57.
[6] Pepley BA, Amphlett JC, Kearns LM, Mann RF. Methanol steam reforming on $Cu/ZnO/Al_2O_3$ catalysts". Part.2. A comprehensive kinetic model. Appl Catal A Gen 1999;179:31–49.
[7] Shishido T, Yamamoto Y, Morioka H, Takaki K, Takehira K. Active Cu/ZnO and $Cu/ZnO/Al_2O_3$ catalysts prepared by homogeneous precipitation method in steam reforming of methanol. Appl Catal A *Gen* 2004;263:249–53.
[8] Busca G, Costantino U, Marmottini F, Montanari T, Patrono P, Pinzari F, et al. Methanol steam reforming over ex-hydrotalcite Cu–Zn–Al catalysts. Appl Cata A *Gen* 2006;310:70–8.
[9] Cavani F, Trifirò F, Vaccari A. Hydrotalcite-type anionic clays : preparation, properties and aplications. *Catal* Today 1991;11:173–301.
[10] Ginés MJL, Amadeo N, Laborde M, Apesteguia CR. Activity and structure-sensivity of the water-gas shift reaction over Cu–Zn–Al mixed oxide catalysts. Appl Catal A *Gen* 1995;131:283–96.
[11] Debecker DP, Gaigneaux EM, Busca G. Exploring, tuning and exploiting the basicity of hydrotalcites for applications in heterogeneous catalysis. J Chem Eur 2009;15:3920–35.
[12] Gennequin C, Siffert S, Cousin R, Aboukaïs A. Co–Mg–Al hydrotalcite precursors for catalytic total oxidation of volatile organic compounds. Top Catal 2009;52:482–91.
[13] Gennequin C, Cousin R, Lamonier J-F, Siffert S, Aboukaïs A. Toluene total oxidation over Co supported catalysts synthesized using "memory effect" of Mg–Al hydrotalcite. Cat Comm 2008;9:1639–43.
[14] Brindley GW, Kikkawa S. A crystal-chemical study of Mg,Al and Ni, N hydroxy-perchlorates and hydroxyl-carbonates. Amer. Min 1979;64:836–43.

[15] Miyata S. The syntheses of hydrotalcite-like compounds and their structures and physico-chemical properties I: the systems MgZ^{+}–Al^{3+}–NO_3, MgZ^{+}–Al^{3+}–Cl^{-}, Mg^{2+}–Al^{3+}–ClO_4^{-}, Ni^{2+}–Al^{3+}–Cl^{-} and Zn^{2+}–Al^{3+}–Cl^{-}. Clays Clay Miner 1975;13:369–75.

[16] Bish DL. Anion-exchange in takovite: applications to other hydroxide minerals. Bull Mineral 1980;103:170–5.

[17] Miyata S. Anion-exchange properties of hydrotalcite-like compounds. Clays Clay Miner 1983;31:305–11.

[18] Gennequin C, Barakat T, Tidahy HL, Cousin R, Lamonier J-F, Aboukaïs A, et al. Use and observation of the hydrotalcite "memory effect" for VOC oxidation. Catal Today 2010;157:191–7.

[19] Montanari T, Sisani M, Nocchetti M, Vivani R, Concepcion Herrera Delgado M, Ramis G, et al. Zinc–aluminum hydrotalcites as precursors of basic catalysts: preparation, characterization and study of the activation of methanol. Catal Today 2010;152:104–9.

[20] Andres Verges M, Mifsud A, Serna CJ. Formation of rod-like zinc oxide microcrystals in homogeneous solutions. J Chem Soc Faraday Trans 1990;86:959–63.

[21] Busca G. Use of infrared spectroscopy methods in the field of heterogeneous catalysts by metal oxides. In: Jackson SD, Hargreaves JSJ, editors. Metal oxide catalysis, vol. 1. Wiley–VCH; 2009. p. 95–175.

[22] Frost RL, Ding Z, Martens WN, Johnson TE, Theo Kloprogge J. Molecular assembly in synthesised hydrotalcites of formula $CuxZn_{6-x}Al_2(OH)_{16}(CO_3)\cdot 4H_2O$—a vibrational spectroscopic study. Spectrochim Acta Part A 2003;59:321–8.

[23] White WB. In: Farmer VC, editor. The infrared spectra of minerals. London: The Mineralogical Society; 1974. p. 226 [Chapter 12].

[24] Pascale F, Tosoni S, Zicovich-Wiklson C, Ugliengo P, Orlando R, Dovesi R. Vibrational spectrum of brucite, $Mg(OH)_2$: a periodic ab initio quantum mechanical calculation including OH anharmonicity. Chem Phys Lett 2004;39:308–15.

[25] Turco M, Bagnasco G, Costantino U, Marmottini F, Montanari T, Ramis G, et al. Production of hydrogen from oxidative steam reforming of methanol: I. Preparation and characterization of $Cu/ZnO/Al_2O_3$ catalysts from a hydrotalcite-like LDH precursor. J Catal 2004;228:43–55.

[26] Frost RL, Martens WN, Erickson KL. Thermal decomposition of the hydrotalcite $Zn_6Al_2CO_3(OH)_{16}\cdot 4H_2O$ – a thermogravimetric analysis and hot stage Raman spectroscopic study. J Therm Anal Calorim 2005;82(3):603–8.

[27] Benito P, Guinea I, Labajos FM, Rocha J, Rives V. Microwave-hydrothermally aged Zn, Al hydrotalcite-like compounds: influence of the composition and the irradiation conditions. Microporous Mesoporous Mater 2008;82:292–302.

[28] Pérez-Ramirez J, Mul G, Moulijn JA. In situ Fourier transform infrared and laser Raman spectroscopic study of the thermal decomposition of Co–Al and Ni–Al hydrotalcites. Vib Spectrosc 2001;27:75–8.

[29] Yang W, Kim Y, Liu PKT, Sahimi M, Tsotsis TT. A study by in situ techniques of the thermal evolution of the structure of a Mg–Al–CO_3 layered double hydroxide. Chem Eng Sci 2002;57:2945–53.

[30] Uzio D. Analyse physico-chimique des catalyseurs industriels. Editions TECHNIP; 2001, ISBN 2-7108-0750-5. p. 6–19. Chapitre 1.

[31] kannan S, Rives V, Knözinger H. High-temperature transformations of Cu-rich hydrotalcites. J Solid State Chem 2004;177:319–31.

[32] Behrens M, Kasatkin I, Kühl S, Weinberg G. Phase-pure Cu,Zn,Al hydrotalcite-like materials as precursors for copper rich $Cu/ZnO/Al_2O_3$ catalysts. Chem Mater 2010;22:386–97.

[33] Goldsmith JA, Ross SD. The infra- red spectra of azurite and malachite. Spectrochim Acta 1968;24A:2131–7.

[34] Atake I, Nishida K, Li D, Shishido T, Oumia Y, Sano T, et al. Catalytic behavior of ternary $Cu/ZnO/Al_2O_3$ systems prepared by homogeneous precipitation in water-gas shift reaction. J Mol Catal A Chem 2007;275:130–8.

[35] Fierro G, Lo Jacono M, Inversi M, Porta P, Cioci F, Lavecchia R. Study of the reducibility of copper in CuO–ZnO catalysts by temperature-programmed reduction. Appl Catal A *Gen* 1996;137:327–48.

[36] Porta P, Dragone R, Lo Jacono M, Minelli G, Moretti G. The reduction process of copper-zinc oxide (alumina) methanol catalysts. Solid State Ionics 1989;32/33:1019–24.

[37] Moretti G, De Rossi S, Ferraris G. Characterization of well dispersed copper species on the surface of ZnO by X-ray photoelectron spectroscopy. Appl Surf Sci 1990;45:341–9.

[38] Velu S, Suzuki K, Okazaki M, Kapoor MP, Osaki T, Ohashi F. Oxidative steam reforming of methanol over CuZnAl(Zr)-oxide catalysts for the selective production of hydrogen for fuel cells: catalyst characterization and performance evaluation. J Catal 2000;194:373–84.

[39] Idem RO, Bakhshi N. Production of hydrogen from methanol. 2. Experimental studies. Ind Eng Chem Res 1994;33:2056–65.

[40] Lwin Y, Daud WRW, Mohamad AB, Yaakob Z. Hydrogen production from steam-methanol reforming: thermodynamic analysis. Int J Hydrogen Energy 2000;25:47–53.

[41] Santacesaria E, Carrà S. Kinetics of a catalytic steam reforming of methanol in a CSTR reactor. Appl Catal 1983;5:345–58.

[42] Geissler K, Newson E, Vogel F, Truong TB, Hottinger P, Wokaum A. Authothermal methanol reforming for hydrogen production in fuel cell applications. Phys Chem Chem Phys 2001;3:289–93.

[43] Agrell J, Birgersson H, Boutonnet M. Steam reforming of methanol over a $Cu/ZnO/Al_2O_3$ catalyst: a kinetic analysis and strategies for suppression of CO formation. J Power Sources 2002;106:249–57.

[44] Peppley BA, Amphlett JC, Kearns LM, Mann RF. Methanol-steam reforming on $Cu/ZnO/Al_2O_3$. Part 1: the reaction network. Appl Catal A *Gen* 1999;179:21–9.

[45] Jiang CJ, Trimm DL, Wainwright MS. Kinetic mechanism for the reaction between methanol and water over a Cu–ZnO–Al_2O_3 catalyst. Appl Catal A Gen 1993;97:145–58.

[46] Jiang CJ, Trimm DL, Wainwright MS. Kinetic study of steam reforming of methanol over copper-based catalysts. Appl Catal 1993;93:245–55.

[47] Breen JP, Ross JRH. Methanol reforming for fuel-cell applications: development of zirconia-containing Cu–Zn–Al catalysts. Catal Today 1999;51:521–33.

[48] Hussein GAM, Sheppard N, Zaki MI, Fahim RB. Infrared spectroscopic studies of the reactions of alcohols over group IVB metal oxide catalysts. 2. Methanol over TiO_2, ZrO_2 and HfO_2. J Chem Soc Faraday Trans 1991;87:2655–9.